HHS Public Access

Author manuscript

Dev Dyn. Author manuscript; available in PMC 2020 April 04.

Published in final edited form as:

Dev Dyn. 2020 April ; 249(4): 573–585. doi:10.1002/dvdy.136.

Phosphotungstic acid enhanced microCT: optimized protocols for embryonic and early postnatal mice

Kate M. Lesciotto[1], **Susan M. Motch Perrine**[1], **Mizuho Kawasaki**[1], **Timothy Stecko**[2], **Timothy M. Ryan**[1], **Kazuhiko Kawasaki**[1], **Joan T. Richtsmeier**[1]

[1]Department of Anthropology, Pennsylvania State University, University Park, PA, USA

[2]Center for Quantitative Imaging, Pennsylvania State University, University Park, PA, USA

Abstract

Background: Given the need for descriptive and increasingly mechanistic morphological analyses, contrast-enhanced microCT represents perhaps the best method for visualizing 3D biological soft tissues *in situ*. While staining protocols using phosphotungstic acid (PTA) have been published with beautiful visualizations of soft tissue structures, these protocols are often aimed at highly specific research questions and are applicable to a limited set of model organisms, specimen ages, or tissue types. We provide detailed protocols for micron-level visualization of soft tissue structures in mice at several embryonic and early postnatal ages using PTA-enhanced microCT.

Results: Our protocols produce microCT scans that enable visualization and quantitative analyses of whole organisms, individual tissues, and organ systems while preserving 3D morphology and relationships with surrounding structures, with minimal soft tissue shrinkage. Of particular note, both internal and external features of the murine heart, lungs, and liver, as well as embryonic cartilage, are captured at high resolution.

Conclusion: These protocols have broad applicability to mouse models for a variety of diseases and conditions. Minor experimentation in the staining duration can expand this protocol to additional age groups, permitting ontogenetic studies of internal organs and soft tissue structures within their 3D *in situ* position.

Keywords

x-ray computed tomography; embryonic development; cartilage; 3D visualization

Introduction:

With the discovery that cells and the tissues they form are not passive materials but instead change their behavior in response to biochemical and biomechanical cues, the analysis of morphology moves from descriptive to mechanistic. As we learn more about the potential for tissue dynamics to influence cell behavior, our need for improved ways to visualize,

Corresponding authors: Kate Lesciotto, Department of Anthropology, Pennsylvania State University, 409 Carpenter Building, University Park, PA 16802, kjl5444@psu.edu, Joan T. Richtsmeier, Department of Anthropology, Pennsylvania State University, 409 Carpenter Building, University Park, PA 16802, jta10@psu.edu.

quantify, and model developing tissues increases. Studies in organismal and structural biology have continuously relied upon various imaging techniques to enable direct visualization of internal and oftentimes microscopic biological structures. Histology provides intricately detailed views of organisms down to the cellular and subcellular level, but with a few exceptions, these studies are limited to two dimensions. Computed tomography (CT) and magnetic resonance imaging (MRI) were developed to answer clinical questions that required an understanding of anatomy and morphology in a 3D context for diagnostic and treatment purposes, with advances in these imaging modalities continuously improving their potential resolutions. These technologies have been eagerly adopted by researchers outside of medicine. One of the most recent advances in imaging adopted by biological scientists outside of medicine is the visualization of microscopic structures using contrast-enhanced microCT, which uses a variety of chemicals to differentially enhance the contrast in x-ray attenuation characteristics of soft tissues (e.g., Descamps et al., 2014; Faulwetter et al., 2012; Metscher, 2011, 2009a, 2009b; Pauwels et al., 2013; Tesařová et al., 2016).

Histology uses thin slices of embedded material that can be stained to highlight different cells or cellular components. A 3D block of biological material must necessarily be destroyed, by embedding the material in a harder substance that enables thin sections (5–15 μm thick) to be produced from the block. The time-consuming process of specimen preparation and sectioning introduces the potential for artifacts that can obscure or distort the tissues and tissue relationships, including tearing, fracturing, or folding of the tissue. A series of 2D histological images may be rendered into an approximation of the original 3D structure only through a labor-intensive process of registering and aligning each image. Even with recent advances in the automation of 3D registration and alignment of serial sections, the process still results in the destruction of the original specimen and can only minimize, but not eliminate, alignment errors and artificial deformations to biological structures (Pichat et al., 2018; Wang et al., 2015). 3D structures and relationships can be visualized in specimens that are cleared and stained, but the clearing process renders the tissue friable, such that continued manipulation during observation can damage anatomical associations and structural relationships.

Both magnetic resonance microscopy (MRM) and microCT allow for the 3D visualization of biological structures. Both procedures are non-destructive with relatively simple protocols, but each has limitations. MRM provides visualization of soft tissue structures, but most MRM systems typically available to researchers provide a resolution of only 40–60 μm. Modern microCT scanners can offer resolutions as low as 1–5 μm, but typically only capture the 3D morphology of mineralized tissues, such as teeth and bone, due to the different x-ray attenuation properties of hard and soft tissues. Phase contrast and synchrotron CT both enable some visualization of soft tissues but are expensive and not as widely available as more traditional microCT systems. Several in-depth reviews summarize the pros and cons of these 3D imaging modalities (e.g., Mizutani and Suzuki, 2012; Norris et al., 2013; Tobita et al., 2010).

Combining microCT with specific staining protocols takes advantage of the increased resolution of microCT and mimics the soft tissue visualization capabilities of MRM. A

number of different chemical stains that enhance contrast in anatomical tissues have been investigated, including osmium tetroxide and phosphomolybdic acid (PMA) (e.g., Descamps et al., 2014; Disney et al., 2017; Kim et al., 2011; Nierenberger et al., 2015), but the majority of the literature has focused on iodine and phosphotungstic acid (PTA) with varying results and recommendations depending upon the model organism, specimen age and size, tissue type, and staining protocol (e.g., De Greef et al., 2015; Degenhardt et al., 2010; Faulwetter et al., 2012; Gignac et al., 2016; Gignac and Kley, 2014; Lautenschlager et al., 2014; Nierenberger et al., 2015; Pauwels et al., 2013; Shearer et al., 2014; Silva et al., 2015; Tsai and Holliday, 2011; Vickerton et al., 2013; Watanabe et al., 2019; Zikmund et al., 2018).

Iodine has emerged as the more popular option, with most published protocols using Lugol's iodine (I_2KI), although some researchers have experimented with iodine in absolute ethanol (I_2E). Iodine has been reported to provide excellent contrast in skeletal muscle, connective, cardiac, and vascular tissues (Degenhardt et al., 2010; Jeffery et al., 2011); however, iodine has been less successful in providing adequate visualization of brain, cartilage, and more collagenous structures (Descamps et al., 2014; Disney et al., 2017; Krings et al., 2017; Lautenschlager et al., 2014; Metscher, 2009a; Tahara and Larsson, 2013, 2013; Tsai and Holliday, 2011). Aside from not staining all tissues equally well, perhaps the most significant drawback to using iodine as a contrast enhancing agent for microCT is the potential for severe tissue shrinkage. Higher concentrations of and prolonged periods of staining with I_2KI, which have been suggested by some as necessary to achieve optimal soft tissue contrast, may result in differential tissue shrinkage rates of up to 70% (Degenhardt et al., 2010; Vickerton et al., 2013). Other studies of larger specimens noted that this extreme degree of shrinkage was not observed, although shrinkage was not specifically quantified (e.g., Gignac & Kley, 2014). One recent study suggests that the high degree of tissue shrinkage may be related to a delay between specimen collection and staining, noting that large *Alligator* and *Gallus* specimens that were immediately fixed and stained following euthanasia did not show evidence of soft tissue shrinkage in the cranium (Watanabe et al., 2019). Balint et al. (2016) report generalized soft tissue shrinkage with morphology altering deformation in iodine-stained porcine ligaments, occurring to a greater extent relative to ligaments stained with either PTA or PMA. Even more recent protocols that involve a tissue-stabilization step prior to iodine staining still note observable tissue shrinkage that may affect morphological analyses (Hsu et al., 2016).

PTA provides an alternate staining option to iodine. PTA is a larger molecule containing tungsten ions and has been recognized as a general stain that particularly emphasizes collagen (Watson, 1958). Early and frequently cited protocols for PTA staining obtained impressive images from a variety of species, including insects, chicken embryos, and mouse embryos; however, the published protocols provided only sparse details (Table 1).

The lack of specific direction for duration of staining necessary for complete penetrance of PTA into soft tissues has resulted in multiple publications, each offering different staining durations with the continuing uncertainty of stain penetrance.

Subsequent to Metscher's published staining protocols (Metscher, 2009a, 2009b, 2011), PTA has been used to visualize soft tissue structures in microCT images of a variety of species

and tissue types, using a multitude of different protocols with varying degrees of success (Table 2). The idea that staining time with PTA was not a critical factor was repeated, so long as staining time was sufficient to penetrate tissues (Nierenberger et al., 2015). However, few details were published that would indicate the length of time needed to sufficiently penetrate tissues of different species and ages. Metscher (2011) suggested that neither the concentration of the PTA staining solution nor the concentration of alcohol was a critical component of the protocol, and a comparison of Metscher's recommended concentration of 0.3% PTA in 70% ethanol with increased concentration (0.6% PTA in 70% ethanol) and increased staining time (overnight versus 10 days at 0.3% PTA) concluded that neither adjustment provided enhanced visualization for any soft tissue types (Krings et al., 2017). Another study tested PTA staining in a marine sponge by increasing the PTA concentration and increasing the incubation temperature to 60°C without success in improving stain penetration (Faulwetter et al., 2012).

One potential advantage of PTA over popular iodine based methods of contrast enhanced microCT is reduced tissue shrinkage during staining. Some studies have used a water-based solution of PTA to avoid shrinkage (Buytaert et al., 2014; De Greef et al., 2015; Descamps et al., 2014). Compared to aqueous and ethanol based iodine solutions, a water-based PTA solution proved to cause the least amount of tissue shrinkage across bone, muscle, and brain tissue samples (Buytaert et al., 2014). Compared to potential deformations in soft tissue morphology resulting from iodine staining (Balint et al., 2016), water-based PTA staining solutions have demonstrated no systematic alteration to osseous and soft tissue structures of middle ear samples, despite the potential for soft tissue shrinkage (De Greef et al., 2015). Ethanol based PTA staining solutions have also reported low rates of shrinkage (Dullin et al., 2017; Krings et al., 2017; Missbach-Guentner et al., 2018). Notably, studies of excised murine hearts and kidneys stained with 0.7% PTA in 70% ethanol actually resulted in a slight swelling of the organs, causing a 9–12% increase in volume, while subsequent chemical drying and embedding procedures resulted in shrinkage and a 7–19% decrease in volume (Dullin et al., 2017; Missbach-Guentner et al., 2018). The concentration of the PTA staining solution likely plays a role in the degree of tissue shrinkage. Using a 10% w/v PTA solution in water to examine porcine tendon resulted in tissue shrinkage of up to 20%, exceeding shrinkage rates for aqueous iodine, although the authors acknowledged that some degree of shrinkage may have resulted from drying that occurred during scanning (Balint et al., 2016). The unusually high concentration of PTA may also have played a role, as the concentration of iodine has been found to contribute to tissue shrinkage. Additional questions have been raised regarding the degree of shrinkage that may result from fixation processes necessary to stabilize and preserve biological specimens (Watanabe et al., 2019).

As shown in Table 2, published protocols for PTA-staining of biological specimens for microCT vary greatly, even when only considering studies examining murine tissues. Variables for staining murine specimens include the concentration of PTA (ranging from 0.7–5%), solution base (water v. ethanol), method of staining (perfusion v. immersion), size of tissue (whole embryo v. excised organ), and staining duration (24 hours up to 18 days). Further, the majority of published protocols provide only minimal details, requiring extensive experimentation to reach an optimized protocol, particularly if using a different model organism, specimen age, or tissue type. One research group has published detailed

PTA protocols for use in embryonic mice from E12.5–18.5 (Kaucka et al., 2017, 2018; Tesařová et al., 2016). The Kaucka and Tesařová protocols added several significant steps to Metscher's (2009a, 2009b) original PTA-staining method: a slow, graded ethanol and methanol dehydration series, different suggested staining times for several ages of embryonic mice, and a final graded methanol rehydration series. The slow dehydration and rehydration steps were added to help minimize soft tissue shrinkage (Kaucka et al., 2017, 2018), addressing many of the concerns with iodine staining. With these modifications, the Kaucka and Tesařová protocols provided excellent contrast enhancement, particularly for embryonic murine cranial soft tissues and cartilage (Kaucka et al., 2017, 2018; Tesařová et al., 2016). However, these protocols vary between publications, making it difficult to elect an optimum method. For example, E15.5 embryos were either stained for 6 days with 0.7% PTA solution (Kaucka et al., 2017; Tesařová et al., 2016) or 3 weeks with 1.0–1.5% PTA solution (Kaucka et al., 2018). These differences may reflect differences in the specific research goals for the stained specimens.

To establish specific protocols for PTA-enhanced microCT that allow for histological, micron-level visualization of soft tissues in both embryonic and early postnatal mice, we adapted and expanded the Kaucka and Tesařová protocols. We present detailed PTA staining protocols that can be used to visualize soft tissues throughout whole embryonic specimens from E13.5 – E15.5, as well as cranial soft tissues in disarticulated heads of specimens from E17.5 through P7. Additionally, we provide protocols for mounting specimens to minimize motion artifacts and desiccation during microCT scanning that allow for the acquisition of initial rapid scans to safeguard against inadequate stain penetration. These protocols explicitly address many of the factors that would otherwise require time-consuming and expensive optimization experiments and permit the study of individual organs and tissues in their natural 3D context. These protocols can be used or adapted by any anatomist, developmental biologist, or morphologist for the study of contrast-enhanced microCT of any mouse model.

Results and Discussion:

Our protocol combines graded alcohol dehydration and rehydration series with an extended duration of staining using 0.7% PTA in 90% methanol for both whole murine specimens (E13.5 – E15.5) and disarticulated heads of late prenatal and early postnatal mice (E16.5 – P7) (Figure 1; see Experimental Procedures for details). This protocol is proven to produce microCT scans with histological-quality level of detail for most soft tissue structures (Figures 2 and 3). Our observations on segmentation and visualization of specific organs and tissues are detailed below.

Brain

Both iodine and PMA have been reported to inadequately stain the brain and associated structures within the endocranial cavity (Degenhardt et al., 2010; Gignac et al., 2016; Lautenschlager et al., 2014; Tsai & Holliday, 2011). Additionally, iodine protocols have reported shrinkage that results in spacing and separation between the skull and brain (Hsu et al., 2016). PTA's ability to successfully stain the brain and permit specific layer

identifications was recognized early by Metscher (2009a) and has further proven to provide superior contrast enhancement and definition of brain regions in a bumblebee, which far exceeded that provided by iodine (Smith et al., 2016).

Figures 3 and 4 show the murine brain in an ontogenetic series from E15.5 to P7. Individual 2D slice images show clear differentiation of various brain regions and tissue layers. These clear boundaries permit the segmentation, quantification, and analysis of both the brain and the ventricular system. In contrast to the iodine protocol used by Hsu et al. (2016), our protocol produces specimens in which the brain remains closely approximated with the skull, suggesting a reduced degree of tissue shrinkage and/or lack of deformation of the brain.

Cartilage

The lack of an appropriate contrast-enhancing microCT stain has hampered investigations into the 3D nature of developing cartilage, particularly in an embryonic context. Cartilage has been reported to stain poorly with iodine (Gignac et al., 2016) and with PTA (Descamps et al., 2014; Krings et al., 2017; Metscher, 2009a). In fact, cartilage has reportedly stained so poorly with PTA as to appear black or like “gaps” in individuals image slices or in volume renderings (Krings et al., 2017; Metscher, 2009a). Others have reported that, while PTA may provide contrast staining of cartilage, PTA is not the optimal choice and may not fully penetrate into calcified cartilage (Krings et al., 2017; Nieminen et al., 2015).

A specific goal of our staining procedure was to visualize embryonic cranial cartilage. Prior to mineralization of cranial bones, the chondrocranium is initially composed only of cartilage and forms to protect the brain and principle sensory organs during embryological development (Kawasaki & Richtsmeier, 2017). Parts of the chondrocranium become mineralized via endochondral ossification while other parts dissolve as they are replaced by dermal bone. Analysis of the early development of the chondrocranium and its association with the forming skull has been hampered by the difficulty in visualizing embryonic cartilage in 3D. The recent Kaucka and Tesařová protocols demonstrated that PTA staining could successfully be used to visualize and analyze the chondrocranium, both in its entirety and with specific focus on the nasal capsule, in embryonic mice (Kaucka et al., 2017, 2018; Tesařová et al., 2016). Our expansion of the Kaucka and Tesařová protocols allows the segmentation of bone from the same PTA-enhanced microCT scan, allowing the creation of high resolution 3D models of the forming dermatocranium and chondrocranium (Figure 5).

Internal Organs

PTA staining has been used on both embryonic and adult mice to visualize internal organ systems, including the heart and kidneys (Dullin et al., 2017; Dunmore-Buyze et al., 2014; Missbach-Guentner et al., 2018). Our protocol builds upon these advances, permitting *in situ* study of these and other developing embryonic organs. In particular, figure 6 demonstrates the high degree of contrast produced by our PTA staining protocol within the heart, lungs, and liver. While some soft tissue shrinkage is evident (Figure 6, white arrows), this protocol allows for detailed 3D reconstructions of external, as well as internal, organ morphology. These protocols preserve spaces within internal organs showing interior details of heart

chambers, vasculature within the developing liver, and bronchial branching patterns of the lungs (Figure 6).

Our protocol improves upon existing procedures by addressing a number of potentially problematic issues with contrast-enhanced microCT. Numerous studies have reported PTA to be a less than ideal staining option, particularly as compared with iodine, due to slower diffusion time through tissues, requiring a longer staining time (Balint et al., 2016). As a larger molecule, PTA will necessarily require longer staining protocols to permit full penetration into deeper tissue structures. Dullin et al. (2017) suggested that the faster diffusion and penetration rates of iodine may decrease image clarity by causing blurring between tissue interfaces. The lower diffusion rate of PTA due its larger molecular size may contribute to the improved edge contrast between tissues (see Figure 6). Although a number of publications have noted that PTA will not penetrate tissues further than a few millimeters deep (Faulwetter et al., 2012; Metscher, 2009b, 2011; Pauwels et al., 2013), an extended staining duration results in the visualization of soft tissues throughout specimens of substantially larger size, overcoming issues related to slower diffusion times.

Higher concentrations of staining solution and longer staining durations are options for improving tissue contrast but often result in increased tissue shrinkage and potential deformation (Degenhardt et al., 2010; Descamps et al., 2014; Gignac & Kley, 2014). Our protocol utilizes a relatively low concentration of PTA (0.7%), extended staining duration, and gradual alcohol dehydration and rehydration steps as suggested in the Kaucka and Tesařová protocols to produce a high degree of contrast between soft tissue structures with a limited amount of shrinkage. To examine the degree of shrinkage, we acquired images of an unstained specimen and then, after staining, acquired a second microCT scan. Superimposition of the two scans enabled estimation of the degree of shrinkage. Assuming that shrinkage is equal in all three dimensions, we estimate an average decrease in size of approximately 10–12% in PTA-stained specimens, significantly less than the shrinkage rates previously published for iodine and comparable or less than published shrinkage rates for PTA (Balint et al., 2016; Buytaert et al., 2014; Degenhardt et al., 2010; Dullin et al., 2017; Missbach-Guentner et al., 2018; Vickerton et al., 2013).

The Kaucka and Tesařová protocols use a gradual dehydration process to avoid abrupt changes to tissues, and the combination of the dehydration series and methanol-based staining solution has proven to provide superior visualization of hollow cavities and spaces within organs and vasculature (Figure 6). Although graded ethanol serial dehydration prior to staining may result in tissue shrinkage, ethanol has been shown to improve phase contrast within soft tissue structures, in part due to evaporation, leaving cavities hollow and providing greater differentiation between the encompassing tissue and spaces within (Dudak et al., 2016). Ethanol-based staining solutions have been further shown to enhance tissue contrast while still minimizing shrinkage effects (Tahara & Larsson, 2013). With an estimated shrinkage rate of approximately 10–12%, our protocol represents an optimized balance between the beneficial phase-contrast improvements of alcohol dehydration with the unavoidable risk of tissue shrinkage. Further, standard histological processing also often involves ethanol dehydration steps, indicating that anatomical and morphological measurements and analyses obtained from PTA-enhanced microCT may not deviate from

similar measurements and analyses performed on histological samples. Some degree of shrinkage appears to be unavoidable with protocols that optimize soft tissue contrast, regardless of the stain (Degenhardt et al., 2010).

Keeping embryos or larger sections of tissue intact, rather than dissecting out individual organs of interest, may also reduce potential shrinkage rates (Baverstock et al., 2013; Tahara & Larsson, 2013; Vickerton et al., 2013). Several studies that have found the largest degree of soft tissue shrinkage for both iodine and PTA based protocols have focused on isolated organs or tissues (Buytaert et al., 2014; Vickerton et al., 2013). In one experiment, *ex vivo* murine brain volume measurements through CT resulted in 60% shrinkage as compared to *in vivo* MRI measurements as a result of fixation with paraformaldehyde (Wehrl et al., 2015). Our protocol allows for whole embryos from E12.5 – E15.5 to remain intact, and although we suggest decapitating heads for late embryonic and early postnatal mice for optimal visualization of cranial soft tissues, several other published protocols have successfully kept postnatal mice entirely intact or with large postcranial portions intact for use with PTA-enhanced microCT (Dullin et al., 2017; Pauwels et al., 2013). Our protocol can be adapted for intact older mice by removing the skin and extending the staining duration.

Critically, our protocol includes an embedding process for scanning that reduces motion artifacts, prevents specimen desiccation, and permits the easy removal of specimens from the embedding matrix without damage. Embedding the samples in agarose or wax has been suggested previously as a method to reduce movement artifacts during scanning (Degenhardt et al., 2010; Dullin et al., 2017; Kaucka et al., 2017, 2018; Metscher, 2011; Missbach-Guentner et al., 2018; Tesařová et al., 2016). Our initial approach used agarose, but removing specimens from agarose embedding, especially embryonic specimens, was difficult and often resulted in damage to the embryo that prevented further analysis or additional scanning of the specimen. Since specimens are often scanned multiple times (e.g., for an initial unstained scan, to check stain penetrance, or improve scan quality), we created a protocol that used an embedding matrix that reduces potential damage during both the embedding and unembedding process. A 50:50 mix of polyester wax and paraffin was found to provide the easiest removal of specimens from wax after scanning without damage, while providing sufficient stability during scanning. By gently heating the embedded specimens in a 70°C water bath, the wax becomes soft enough to peel and flake away from even the most fragile embryonic specimens.

By utilizing the low concentration of PTA over an extended staining duration with a graded alcohol dehydration and rehydration series, our method provides superior visualization of many soft tissue structures in embryonic and early postnatal mice. Importantly, several studies found that PTA stained tissues and specimens could still be utilized for histological or immunohistochemical examination without significant alteration of morphology (Dullin et al., 2017; Missbach-Guentner et al., 2018), indicating that this protocol would not preclude further specimen analysis through other methods. While the specimens used in development and in the figures presented here represent typical phenotypes, this protocol has broad applicability to any number of mouse models for a variety of diseases and conditions. Minor supplemental experimentation in the staining duration should expand this protocol to

additional embryonic and postnatal age groups, permitting ontogenetic studies of internal organs and soft tissue structures within their 3D *in situ* setting. Further experimentation could broaden the application of this protocol across mammalian and non-mammalian species for which microCT studies are becoming more common. For example, this protocol could be combined with PaxGene fixation protocols to both preserve the ability for RNA extraction while improving contrast within soft tissue structures (Green et al., 2017, 2019) or potentially be applied to non-mammalian species in which contrast-enhanced microCT has been increasingly utilized to study development of soft tissue structures (Faulwetter et al., 2012, Smith et al., 2016, Swart et al., 2016, Theodosiou et al., 2018). Overall, the combination of detailed protocols for staining tissues with PTA and wax-embedding to minimize tissue shrinkage and movement artifacts during scanning has broad applications.

Experimental Procedures:

Mice were produced, sacrificed, and processed in compliance with animal welfare guidelines approved by the Pennsylvania State University Animal Care and Use Committee (IBC# 48199). Based upon timed mating and evidence of pregnancy, litters were sacrificed and collected on embryonic days (E) 13.5, 14.5, 15.5, 16.5, and 17.5. Postnatal (P) litters were only used if birth occurred on post-conception day 19 for mice on a C57BL/6J background and were collected on the day of birth (P0) and P7. Pregnant damns and postnatal pups were euthanized by inhalation anesthetics, and heads of postnatal pups were disarticulated at the cervical spine. Embryos and postnatal heads were fixed in 4% paraformaldehyde (PFA) in phosphate-buffered saline (PBS), and then stored in PBS with 0.01% sodium azide as an antibacterial agent until ready for staining. After fixation, embryos older than E15.5 were disarticulated at the cervical spine or mid-thorax, depending on the size of the specimen and tissues of interest. Immediately prior to staining, the skin was removed from the postnatal heads, being careful to leave the ears, nasal skin, and lips intact to avoid pulling and distortion of internal structures.

All following procedures were carried out at 4°C, with samples kept on a rocking table. The PTA staining protocol outlined below was adapted from Tesařová et al. (2016) and expanded to include specific staining durations for a number of embryonic and postnatal ages. Importantly, our protocols provide additional instruction based upon the genetic background of the mice. We have found that the larger size of mice bred on a CD1 background (compared to mice bred on a C57BL/6J background) requires a longer staining duration to reach adequate stain penetration and optimum contrast. Once ready to begin the PTA staining process, all samples were taken through a dehydration series outlined below:

1. Samples were washed in PBS for 1 day;
2. 30% ethanol in PBS for 1 day;
3. 50% ethanol in PBS for 1 day;
4. 70% ethanol in ultrapure water for 1 day;
5. 4:4:3 ethanol:methanol:ultrapure water for 1 hour;
6. 80% methanol in ultrapure water for 1 hour; and

7. 90% methanol in ultrapure water for 1 hour.

Following dehydration, samples were immersed in 0.7% PTA (Sigma Aldrich No. P4006–25G) in 90% methanol for the duration indicated in Table 3. Solution was changed daily for all embryonic ages. For postnatal ages, PTA solution was changed daily for the first 10 days and then every other day until the end of the indicated staining duration.

While these staining times have been found to be optimal for the majority of specimens, we found it useful to complete a test scan towards the end of the PTA staining time. Specimens would be placed in small glass vials with PTA staining solution to undergo a rapid microCT scan of only 10–30 minutes, depending on the number of specimens being tested, at low resolution. Keeping specimens in a liquid medium prevents desiccation but increases the risk of movement artifacts. Since these scans were only used to determine stain penetrance and not for analysis, this was deemed acceptable. Scan reconstructions could be quickly reviewed by experienced technicians to determine whether the stain had completely penetrated the specimen and optimum contrast levels had been reached. Depending on the results of these test scans, specimens could either have additional staining days added to the protocol or proceed to the rehydration series.

Once PTA staining was completed, all samples were then rehydrated as follows:

1. 90% methanol in ultrapure water for 6 hours;
2. 80% methanol in ultrapure water overnight;
3. 70% methanol in ultrapure water for 6 hours;
4. 50% methanol in PBS overnight;
5. 30% methanol in PBS for 1 day;
6. PBS for 1 day; and
7. Store in 0.01% sodium azide in PBS until scanning.

While staining does appear to be retained for several weeks, optimum tissue contrast and edge clarity was obtained when specimens were scanned within several days of completing the rehydration series.

Immediately prior to scanning, samples are embedded in a 50:50 mix of polyester and paraffin waxes (Electron Microscopy Sciences Cat#19312 and 19302–01, respectively) to prevent movement artifacts and desiccation (Figure 7). Specimens are removed from the storage solution and gently dried with tissue paper. The 50:50 wax mix is heated to approximately 70°C. Using a pre-heated syringe, roughly 5 mm of the wax mix is injected into the bottom of a piece of small diameter metal or plastic tubing appropriate for the specimen size. Once the base layer of wax solidified, the specimen is dipped gently in liquid wax several times and then placed nose-down within the tube. Dissection tools are used to hold the specimen in place while additional wax is injected in the surrounding space to completely fill the tube. After the wax has solidified, multiple specimens could be layered into a stack for scanning.

MicroCT images were acquired by the Center for Quantitative Imaging at the Pennsylvania State University (www.cqi.psu.edu) using the General Electric v|tom|x L300 nano/microCT system. This is a dual-tube system, with a 300kV microfocus tube for larger specimens and a 180kV nanofocus tube for smaller specimens. Although specimens may be scanned using either tube, we found the greatest resolution and scan quality was typically produced by the 180kV tube for embryonic specimens and the 300kV tube for postnatal specimens. Image data were reconstructed on a 2024 × 2024 pixel grid as a 32bit volume, but may be reduced to 16-bit for image analysis with Avizo 9.4 (Thermo Fisher Scientific) (see Supplemental Video 1). Scanning parameters are provided in Table 4.

Once scanning is completed, specimens are removed from the wax casing by placing each casing in a 50 mL tube in a 70°C water bath. Specimens are checked every 2 minutes, and once the wax begins to soften, the wax can be gently peeled away from the specimen using dissection probes and forceps. Specimens are then placed back into PBS with 0.01% sodium azide.

The gentle nature of the wax embedding permits multiple rounds of scanning without damage to the specimen. For example, for studies that wish to examine the relationship between bone and underlying soft tissues, this protocols permits an initial unstained scan optimized to capture bone and mineralized tissues, followed by PTA-staining and a subsequent scan of the same specimen, now optimized to capture soft tissues, as outlined above. This procedure enables the superimposition of both scans to capture the 3D relationship between hard and soft tissues in developing mice.

Supplementary Material

Refer to Web version on PubMed Central for supplementary material.

Acknowledgements:

We wish to thank Whitney Yetter at the Center for Quantitative Imaging at the Pennsylvania State University (www.cqi.psu.edu) for her technical expertise and help with the General Electric v|tom|x L300 nano/microCT system.

Grant Support:

- National Science Foundation BCS 1731909
- National Institutes of Health R01DE022988, P01HD078233, and R01DE027677

References:

Balint R, Lowe T, Shearer T. 2016 Optimal contrast agent staining of ligaments and tendons for x-ray computed tomography. PLoS ONE 11:e0153552. [PubMed: 27078030]

Baverstock H, Jeffery NS, Cobb SN. 2013 The morphology of the mouse masticatory musculature. J Anat 223:46–60. [PubMed: 23692055]

Buytaert J, Goyens J, De Greef D, Aerts P, Dirchx J. 2014 Volume shrinkage of bone, brain, and muscle tissue in sample preparation from microCT and LSFM. Microsc Microanal 20:1208–1217. [PubMed: 24963987]

De Greef D, Buytaert JAN, Aerts JRM, Van Hoorebeke L, Dierick M, Dirckx J. 2015 Details of human middle ear morphology based on micro-CT imaging of phosphotungstic acid stained samples: human middle ear morphology through micro-CT. J Morphol 276:1025–1046. [PubMed: 26010747]

Degenhardt K, Wright AC, Horng D, Padmanabhan A, Epstein JA. 2010 Rapid 3D phenotyping of cardiovascular development in mouse embryos by micro-CT with iodine staining. Circ Cardiovasc Imaging 3:314–322. [PubMed: 20190279]

Descamps E, Sochacka A, Kegel BD, Loo DV, Hoorebeke V, Adriaens D. 2014 Soft tissue discrimination with contrast agents using micro-CT scanning. Belg J Zool 144:20–40.

Disney CM, Madi K, Bodey AJ, Lee PD, Hoyland JA, Sherratt MJ. 2017 Visualising the 3D microstructure of stained and native intervertebral discs using X-ray microtomography. Sci Rep 7:16279. [PubMed: 29176563]

Dudak J, Zemlicka J, Karch J, Patzelt M, Mrzilkova J, Zach P, Hermanova Z, Kvacek J, Krejci F. 2016 High-contrast X-ray micro-radiography and micro-CT of ex-vivo soft tissue murine organs utilizing ethanol fixation and large area photon-counting detector. Sci Rep 6:30385. [PubMed: 27461900]

Dullin C, Ufartes R, Larsson E, Martin S, Lazzarini M, Tromba G, Missbach-Guentner J, Pinkert-Leetsch D, Katschinski DM, Alves F. 2017 μCT of ex-vivo stained mouse hearts and embryos enables a precise match between 3D virtual histology, classical histology and immunochemistry. PLoS ONE 12:e0170597. [PubMed: 28178293]

Dunmore-Buyze PJ, Tate E, Xiang F, Detombe SA, Nong Z, Pickering G, Drangova M. 2014 Three-dimensional imaging of the mouse heart and vasculature using micro-CT and whole-body perfusion of iodine or phosphotungstic acid: vascular tissue visualization with perfusion technique. Contrast Media Mol Imaging 9:383–390. [PubMed: 24764151]

Faulwetter S, Dailianis T, Vasileiadou A, Arvanitidis C. 2012 Investigation of contrast enhancing techniques for the application of microCT in marine biodiversity studies. SkyScan MicroCT User Meet 2012:12–20.

Gignac PM, Kley NJ, Clarke JA, Colbert MW, Morhardt AC, Cerio D, Cost IN, Cox PG, Daza JD, Early CM, Echols MS, Henkelman RM, Herdina AN, Holliday CM, Li Z, Mahlow K, Merchant S, Müller J, Orsbon CP, Paluh DJ, Thies ML, Tsai HP, Witmer LM. 2016 Diffusible iodine-based contrast-enhanced computed tomography (diceCT): an emerging tool for rapid, high-resolution, 3-D imaging of metazoan soft tissues. J Anat 228:889–909. [PubMed: 26970556]

Gignac PM, Kley NJ. 2014 Iodine-enhanced micro-CT imaging: methodological refinements for the study of the soft-tissue anatomy of post-embryonic vertebrates. J Exp Zoolog B Mol Dev Evol 322:166–176.

Green RM, Leach CL, Hoehn N, Marcucio RS, Hallgrímsson B. 2017 Quantifying three-dimensional morphology and RNA from individual embryos. Dev Dyn 246:431–436. [PubMed: 28152580]

Green RM, Leach CL, Diewert VM, Aponte JD, Schmidt EJ, Cheverud JM, Roseman CC, Young NM, Marcucio RS, Hallgrímsson B. 2019 Nonlinear gene expression-phenotype relationships contribute to variation and clefting in the A/WySn mouse. Dev Dyn 2019:1–11. 10.1002/dvdy.110

Hsu C-W, Wong L, Rasmussen TL, Kalaga S, McElwee ML, Keith LC, Bohat R, Seavitt JR, Beaudet AL, Dickinson ME. 2016 Three-dimensional microCT imaging of mouse development from early post-implantation to early postnatal stages. Dev Biol 419:229–236. [PubMed: 27671873]

Jeffery NS, Stephenson RS, Gallagher JA, Jarvis JC, Cox PG. 2011 Micro-computed tomography with iodine staining resolves the arrangement of muscle fibres. J Biomech 44:189–192. [PubMed: 20846653]

Kaucka M, Petersen J, Tesařová M, Szarowska B, Kastriti ME, Xie M, Kicheva A, Annusver K, Kasper M, Symmons O, Pan L, Spitz F, Kaiser J, Hovorakova M, Zikmund T, Sunadome K, Matise MP, Wang H, Marklund U, Abdo H, Ernfors P, Maire P, Wurmser M, Chagin AS, Fried K, Adameyko I. 2018 Signals from the brain and olfactory epithelium control shaping of the mammalian nasal capsule cartilage. eLife 7e34465.

Kaucka M, Zikmund T, Tesařová M, Gyllborg D, Hellander A, Jaros J, Kaiser J, Petersen J, Szarowska B, Newton PT, Dyachuk V, Li L, Qian H, Johansson A-S, Mishina Y, Currie JD, Tanaka EM, Erickson A, Dudley A, Brismar H, Southam P, Coen E, Chen M, Weinstein LS, Hampl A, Arenas E, Chagin AS, Fried K, Adameyko I. 2017 Oriented clonal cell dynamics enables accurate growth and shaping of vertebrate cartilage. eLife 6e25902.

Kawasaki K, Richtsmeier JT. 2017 Association of the chondrocranium and dermatocranium in early skull formation In: Building Bones: Bone Formation and Development in Anthropology, (Ed. Percival CJ & Richtsmeier JT), pp. 52–78. Cambridge, UK: Cambridge University Press.

Kim JS, Min J, Recknagel AK, Riccio M, Butcher JT. 2011 Quantitative three-dimensional analysis of embryonic chick morphogenesis via microcomputed tomography. Anat Rec 294:1–10.

Krings M, Müller H, Heneka M, Rödder D.2017 Modern morphological methods for tadpole studies: a comparison of micro-CT, and clearing and staining protocols modified for frog larvae. Biotech Histochem 92:595–605. [PubMed: 29210297]

Lautenschlager S, Bright JA, Rayfield EJ. 2014 Digital dissection - using contrast-enhanced computed tomography scanning to elucidate hard- and soft-tissue anatomy in the Common Buzzard Buteo buteo. J Anat 224:412–431. [PubMed: 24350638]

Metscher BD. 2009a MicroCT for comparative morphology: simple staining methods allow high-contrast 3D imaging of diverse non-mineralized animal tissues. BMC Physiol 9:11. [PubMed: 19545439]

Metscher BD. 2009b MicroCT for developmental biology: a versatile tool for high-contrast 3D imaging at histological resolutions. Dev Dyn 238:632–640. [PubMed: 19235724]

Metscher BD. 2011 X-Ray microtomographic imaging of intact vertebrate embryos. Cold Spring Harb Protoc 12:pdb.prot067033.

Missbach-Guentner J, Pinkert-Leetsch D, Dullin C, Ufartes R, Hornung D, Tampe B, Zeisberg M, Alves F. 2018 3D virtual histology of murine kidneys –high resolution visualization of pathological alterations by micro computed tomography. Sci Rep 8:1407. [PubMed: 29362427]

Mizutani R, Suzuki Y. 2012 X-ray microtomography in biology. Micron 43:104–115. [PubMed: 22036251]

Nieminen HJ, Ylitalo T, Karhula S, Suuronen J-P, Kauppinen S, Serimaa R, Hæggström E, Pritzker KPH, Valkealahti M, Lehenkari P, Finnilä M, Saarakkala S. 2015 Determining collagen distribution in articular cartilage using contrast-enhanced micro-computed tomography. Osteoarthritis Cartilage 23:1613–1621. [PubMed: 26003951]

Nierenberger M, Rémond Y, Ahzi S, Choquet P. 2015 Assessing the three-dimensional collagen network in soft tissues using contrast agents and high resolution micro-CT: application to porcine iliac veins. C R Biol 338:425–433. [PubMed: 26033495]

Norris FC, Wong MD, Greene NDE, Scambler PJ, Weaver T, Weninger WJ, Mohun T, Henkelman RM, Lythgoe MF. 2013 A coming of age: advanced imaging technologies for characterising the developing mouse. Trends Genet 29:700–711. [PubMed: 24035368]

Pauwels E, Van Loo D, Cornillie P, Brabant L, Van Hoorebeke L. 2013 An exploratory study of contrast agents for soft tissue visualization by means of high resolution X-ray computed tomography imaging: contrast agents for soft tissue visualization with microCT. J Microsc 250:21–31. [PubMed: 23432572]

Pichat J, Iglesias JE, Yousry T, Ourselin S, Modat M. 2018 A survey of methods for 3D histology reconstruction. Med Image Anal 46:73–105. [PubMed: 29502034]

Shearer T, Rawson S, Castro SJ, Balint R, Bradley RS, Lowe T, Vila-Comamala J, Lee PD, Cartmell SH. 2014 X-ray computed tomography of the anterior cruciate ligament and patellar tendon. Muscles Ligaments Tendons Journal 4:238–244.

Silva de Se JM, I Zanette, PB Noël, MB Cardoso, MA Kimm, F Pfeiffer. 2015 Three-dimensional non-destructive soft-tissue visualization with X-ray staining micro-tomography. Sci Rep 5:14088. [PubMed: 26404036]

Smith DB, Bernhardt G, Raine NE, Abel RL, Sykes D, Ahmed F, Pedroso I, Gill RJ. 2016 Exploring miniature insect brains using micro-CT scanning techniques. Sci Rep 6:21768. [PubMed: 26908205]

Swart P, Wicklein M, Sykes D, Ahmed F, Krapp HG. 2016 A quantitative comparison of micro-CT preparations in Dipteran flies. Sci Rep 6:39380. [PubMed: 28000717]

Tahara R, Larsson HCE. 2013 Quantitative analysis of microscopic X-ray computed tomography imaging: Japanese quail embryonic soft tissues with iodine staining. J Anat 223:297–310. [PubMed: 23869493]

Tesařová M, Zikmund T, Kaucká M, Adameyko I, Jaros J, Palousek D, Skaroupka D, Kaiser J. 2016 Use of micro computed-tomography and 3D printing for reverse engineering of mouse embryo nasal capsule. J Instrum 11:C03006.

Theodosiou NA, Oppong E. 201903D morphological analysis of spiral intestine morphogenesis in the little skate, Leucoraja erinacea. Dev Dyn 248:688–701. [PubMed: 30938886]

Tobita K, Liu X, Lo CW. 2010 Imaging modalities to assess structural birth defects in mutant mouse models. Birth Defects Res Part C Embryo Today Rev 90:176–184.

Tsai HP, Holliday CM. 2011 Ontogeny of the alligator cartilago transiliens and its significance for sauropsid jaw muscle evolution. PLoS ONE 6:e24935. [PubMed: 21949795]

Vickerton P, Jarvis J, Jeffery N. 2013 Concentration-dependent specimen shrinkage in iodine-enhanced microCT. J Anat 223:185–193. [PubMed: 23721431]

Wang C-W, Gosno EB, Li Y-S. 2015 Fully automatic and robust 3D registration of serial-section microscopic images. Sci Rep 5:15051. [PubMed: 26449756]

Watanabe A, Gignac PM, Balanoff AM, Green TL, Kley NJ, Norell MA. 2019 Are endocasts good proxies for brain size and shape in archosaurs throughout ontogeny? J Anat 234:291–305. [PubMed: 30506962]

Watson ML. 1958 Staining of tissue sections for electron microscopy with heavy metals. J Cell Biol 4:475–478.

Wehrl HF, Bezrukov I, Wiehr S, Lehnhoff M, Fuchs K, Mannheim JG, Quintanilla-Martine L, Kohlhofer U, Kneilling M, Pichler BJ, Sauter AW. 2015 Assessment of murine brain tissue shrinkage caused by different histological fixatives using magnetic resonance and computed tomography imaging. Histol Histopathol 30:601–613. [PubMed: 25504583]

Zikmund T, Novotná M, Kavková M, Tesařová M, Kaucka M, Szarowska B, Adameyko I, Hruba E, Buchtova M, Drazanova E, Starcuk Z, Kaiser J. 2018 High-contrast differentiation resolution 3D imaging of rodent brain by X-ray computed microtomography. J Instrum 13:C02039.

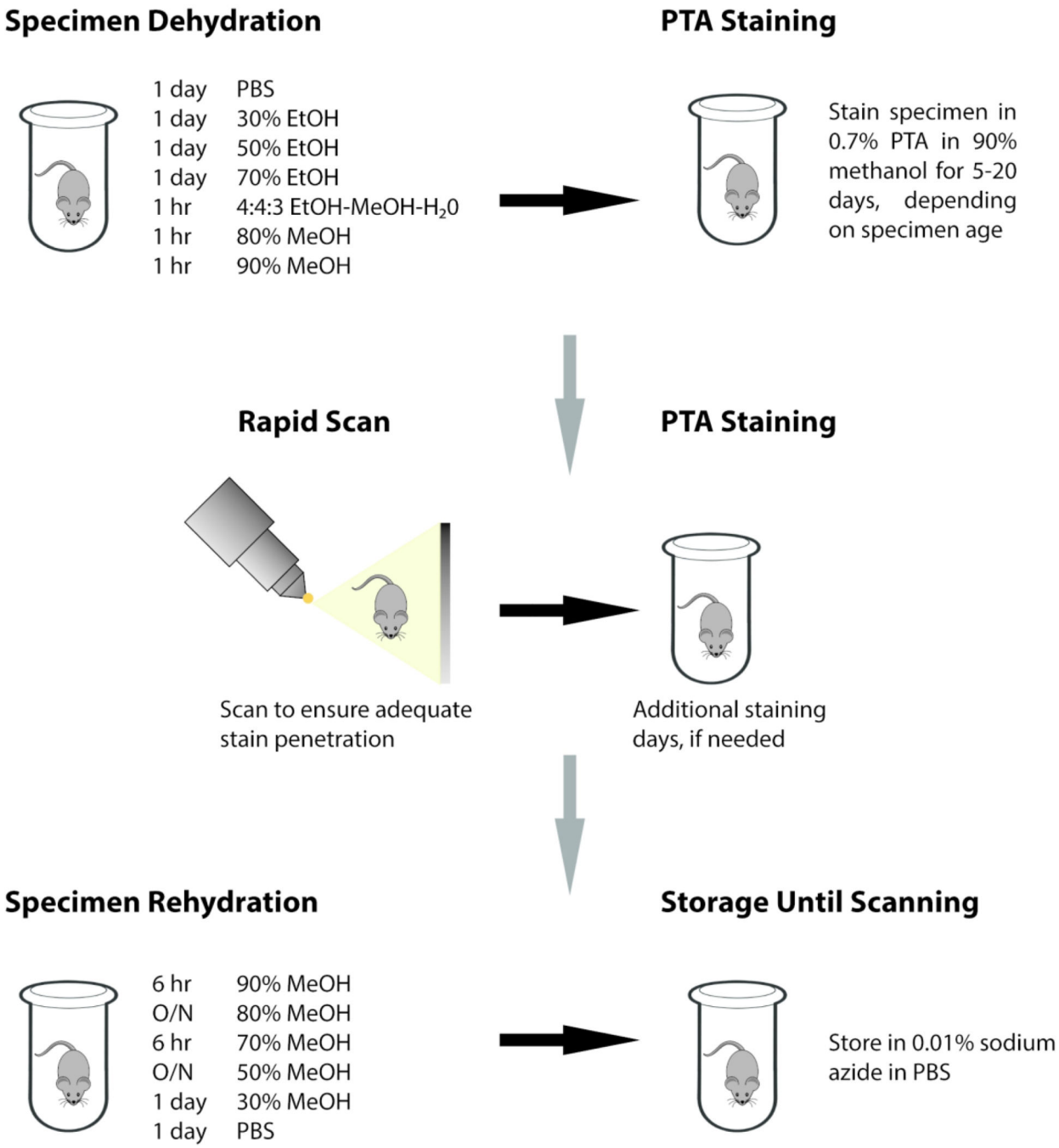

Figure 1.
Illustration of PTA staining protocol.

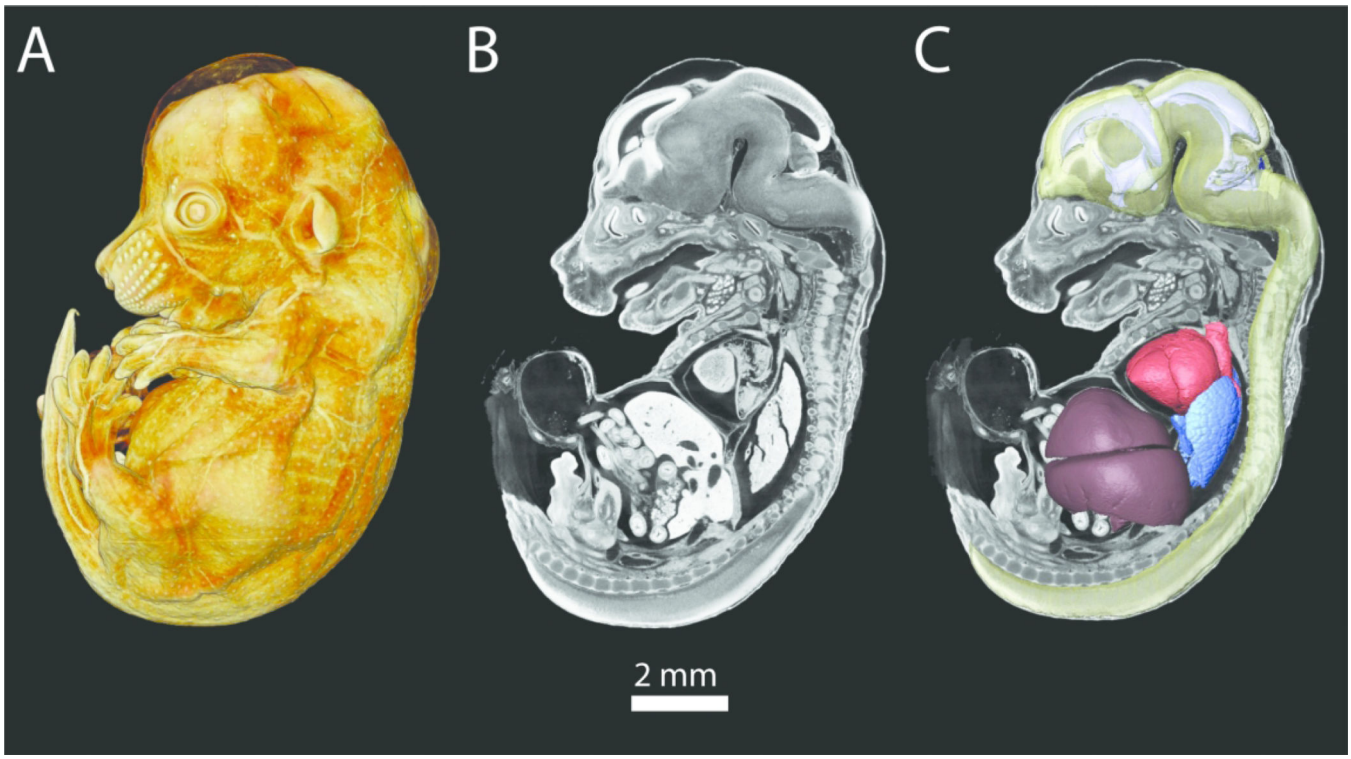

Figure 2.

A PTA-stained E14.5 mouse embryo scanned at a resolution of 6 microns. *A)* Volume rendering of whole PTA stained embryo. *B)* 2D parasagittal slice of PTA stained embryo. *C)* Same slice as in B, with 3D reconstructions of the brain and spinal cord (transparent yellow), ventricular system (pale purple), heart (red), lungs (blue), and liver (deep purple).

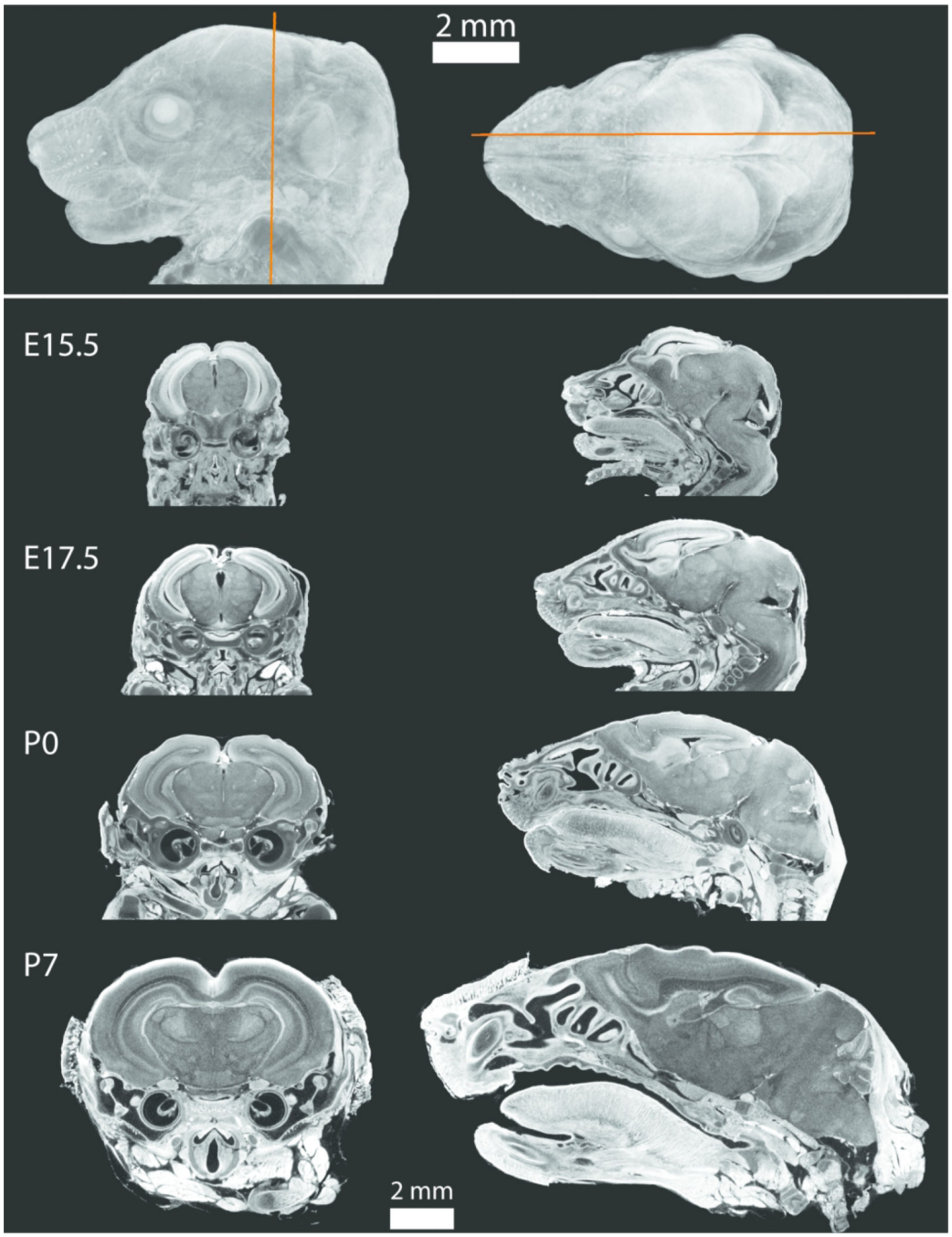

Figure 3.

Volume rendering of an E17.5 mouse (top) showing the approximate location of the coronal (left) and parasagittal (right) 2D slices of PTA-stained scanned specimens for four developmental ages (bottom). Voxel sizes for each scan were 0.006 mm for E15.5, 0.007 mm for E17.5 and P0, and 0.011 mm for P7, and all 2D slices are shown in the same scale. Note the close association between the brain and developing skull, indicating reduced tissue shrinkage.

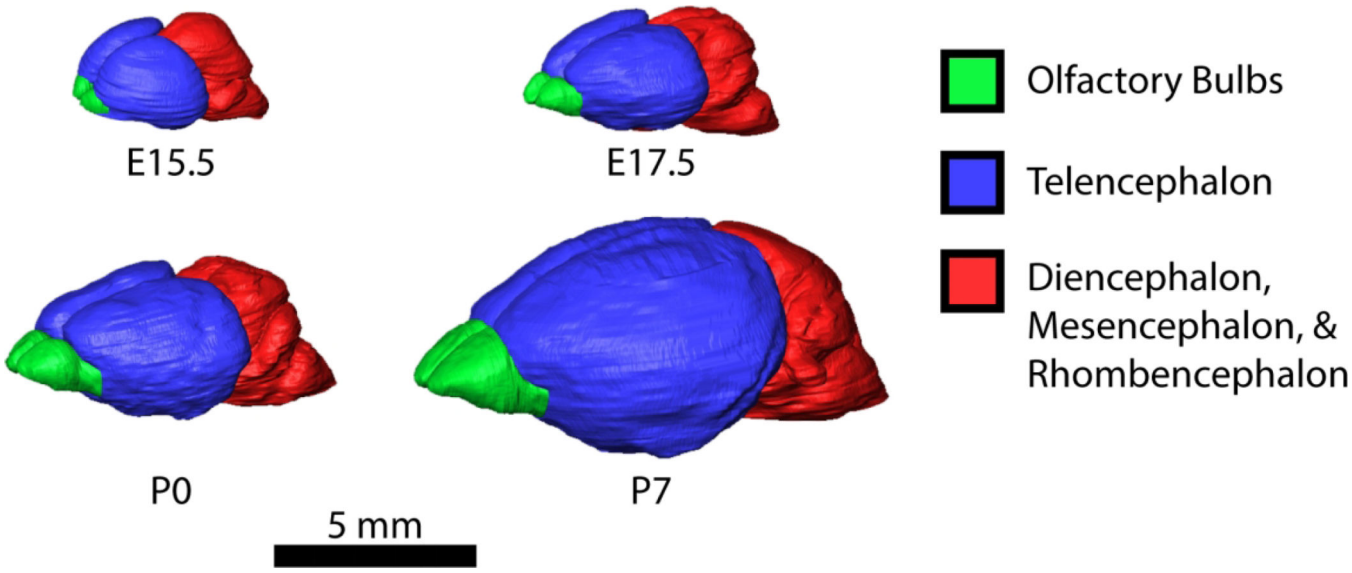

Figure 4.

3D reconstructions of mouse brains shown to scale at E15.5, E17.5, P0, and P7. Reconstructions were created in Avizo 9.4, using the segmentation editor. Brain regions were manual segmented at every 5–10 slices and the interpolated for the intervening slices.

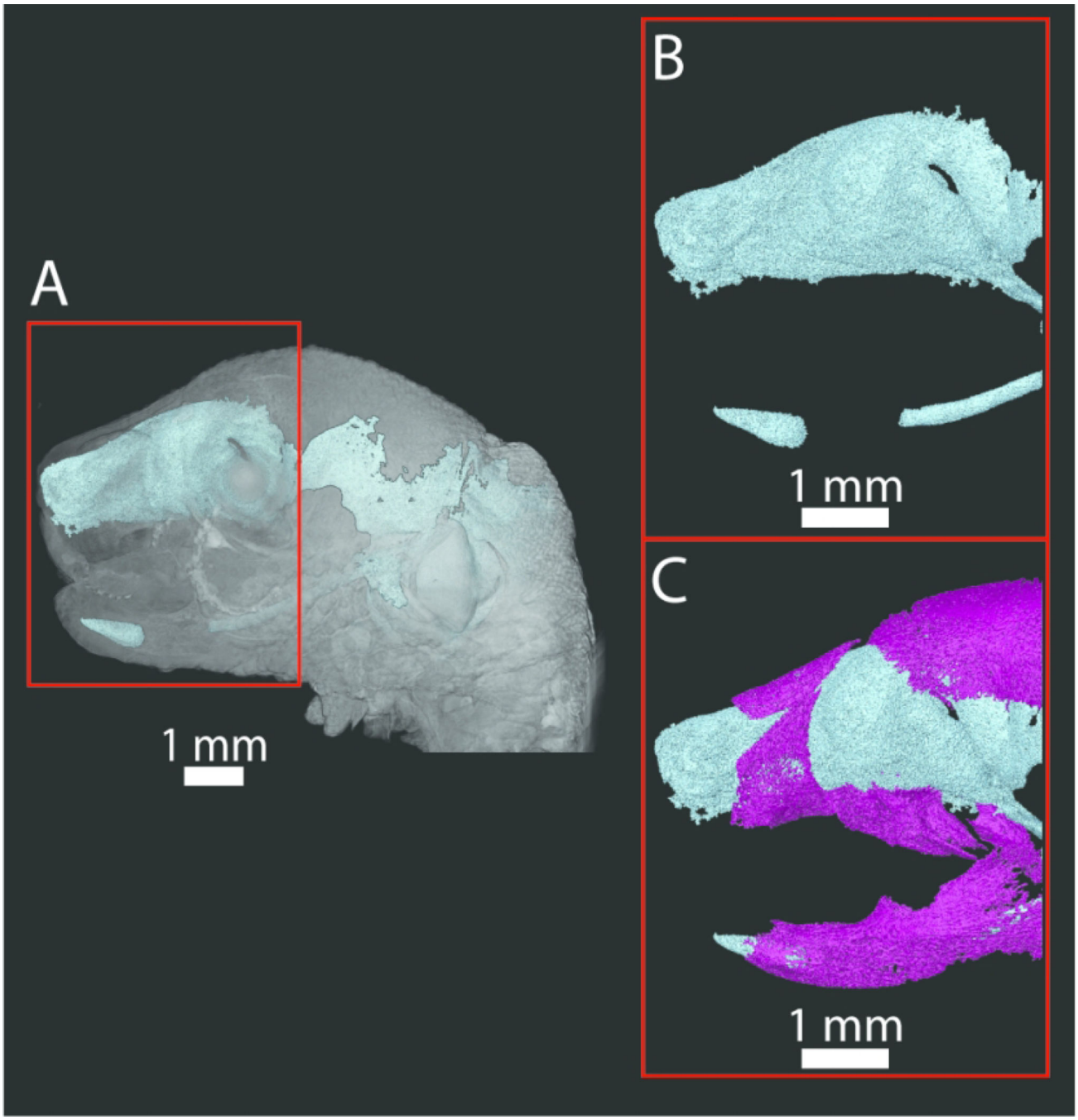

Figure 5.

A) Volume rendering of the PTA-stained head of an E17.5 CD1 mouse (surface in gray) and 3D reconstruction of the chondrocranium and Meckel's cartilage (teal). Red box indicates the area of enlargement in B and C. Note that no smoothing algorithms were used in order to present the raw data. *B)* Enlargement of the anterior portion of the chondrocranium (including the nasal capsule and ala orbitalis) and Meckel's cartilage (teal). *C)* Addition of bone (nasal bones, premaxilla, maxilla, frontal, above and dentary, below) (magenta) segmented from the same PTA-stained scan, showing the relationship between the

chondrocranium and Meckel's cartilage and forming bone. Incisors are developing within their crypts at this stage.

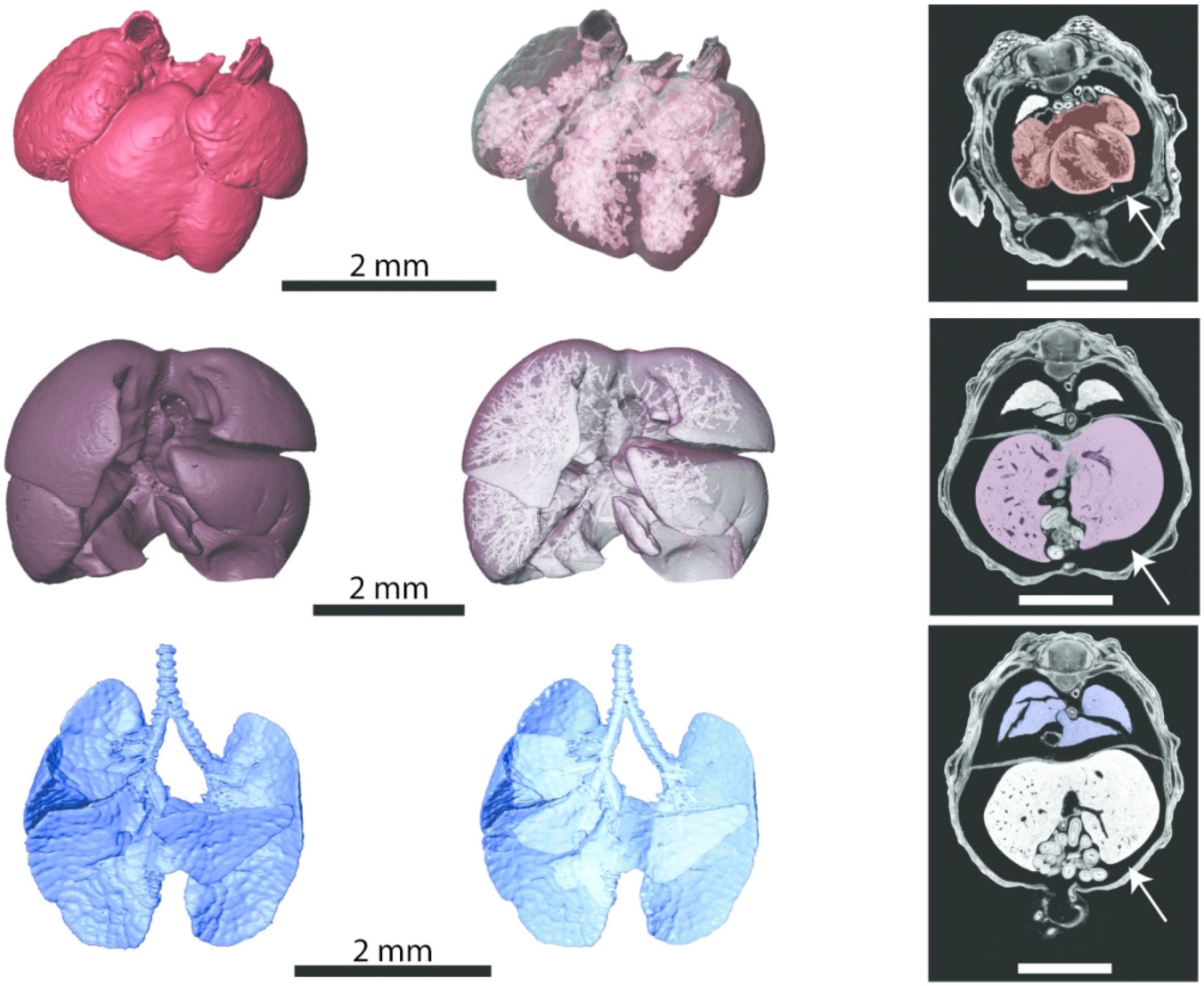

Figure 6.

Heart (top row), liver (middle row), and lungs (bottom row) of an E14.5 C57BL/6J mouse embryo scanned at a resolution of 0.006 mm. Left column: Anterior views of 3D reconstructions of the organs. Middle column: Anterior views of 3D reconstructions of the organs made transparent to visualize the spaces with the organs. Right column: Individual 2D transverse slices from the microCT scan, with the heart shaded in red, liver shaded in purple, and lungs shaded in blue. White arrows indicate spaces between the organs and body wall, indicating soft tissue shrinkage. All scale bars are 2 mm.

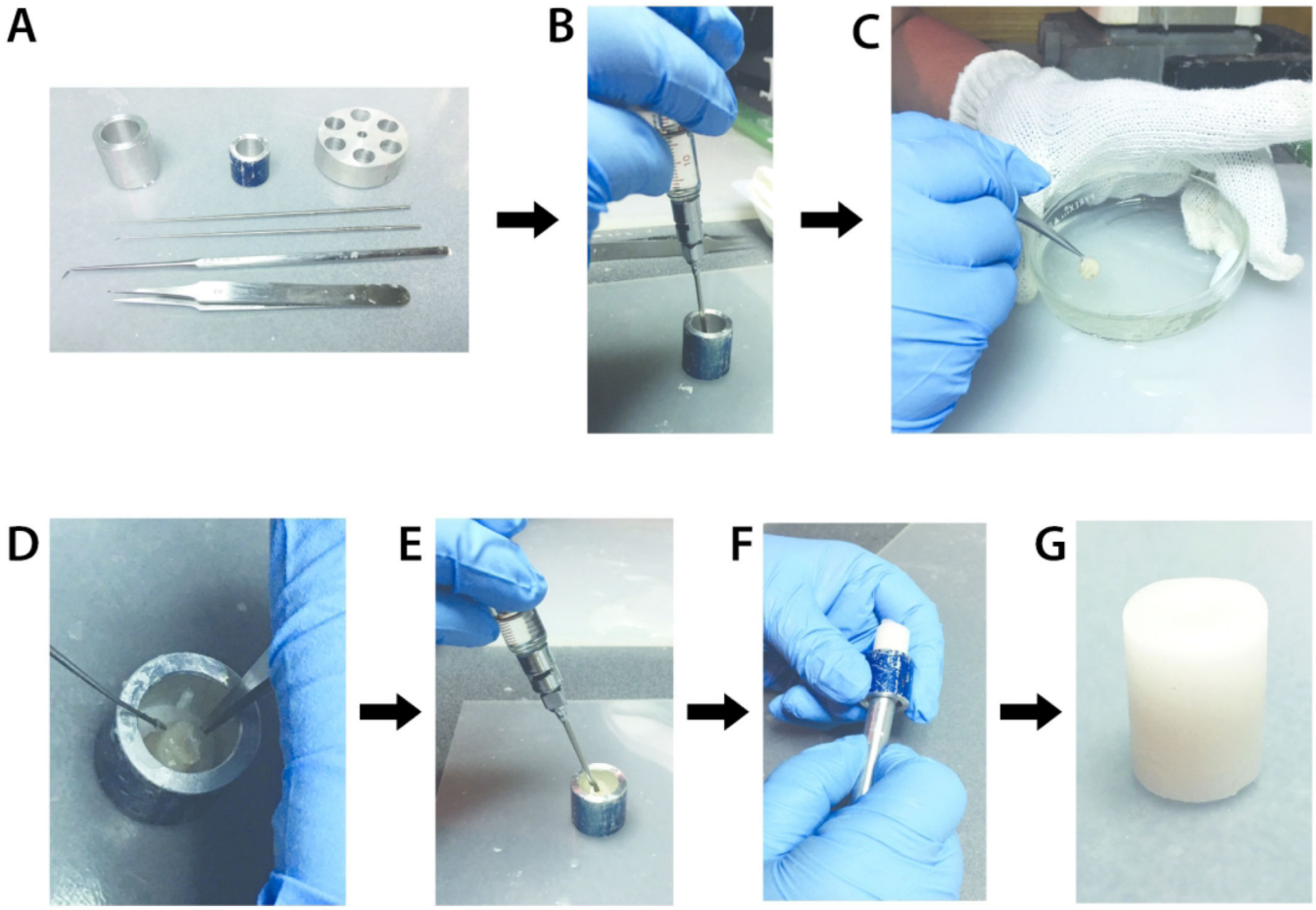

Figure 7.

Process for embedding a specimen in wax for scanning. A) Tools used during the embedding process, including several sizes of tubes and dissection tools. B) A 5 mm layer of the 50:50 wax mix is injected into the bottom of a metal tube using a syringe preheated to 70°C. C) The specimen is gently dipped in the wax mix five times. D) The specimen is placed nose down into the tube, on top of the 5 mm base layer of wax mix. E) Additional wax mix is injected to completely surround the specimen. F) Once the wax mix has fully solidified (approximately 5–7 minutes), the sample is gently pushed out of the metal case. G) The final sample of an E17.5 specimen embedded in wax and ready for scanning.

Table 1.

Summary of early PTA-staining protocols.

Reference	Ethanol dehydration	PTA Staining	Notes
(Metscher, 2009a)	"Take samples to 70% ethanol."	0.3% PTA in 70% ethanol "Stain overnight or longer."	"The staining times were found not to be critical, as long as the stain had sufficient time to penetrate the tissues."
(Metscher, 2009b)	"Samples in 70% ethanol."	0.3% PTA in 70% ethanol "Stain 2 hr to overnight."	"Slow tissue penetration, limited to a few millimeters."
(Metscher, 2011)	"Rinse in water. Transfer to 35% ethanol and leave for 10–15 min. Transfer to 70% ethanol and leave for 10–15 min or longer."	0.3% PTA in 70% ethanol "Stain in PTA for 2 h to overnight."	"The staining time is not critical and PTA does not overstain, but larger embryos (e.g., E12 or later mice) should be stained overnight. PTA has trouble penetrating more than about 2 mm of tissue." "The PTA concentration is not critical, nor is the grade and concentration of alcohol."

Table 2.

Survey of PTA staining protocols published after Metscher 2009a, b, and 2011.

Reference	Species	Age	Tissues	Staining Solution	Staining duration
(Descamps et al., 2014)	Mouse	E14.5	Whole body	2.5% PTA in demineralized water	24 hrs
(Balint et al., 2016)	Pig	Not reported	Ligaments and tendons	10% w/v PTA in water	Up to 5 days
(Buytaert et al., 2014)	Rabbit	12 wk	Bone, muscle, nerve, fat	0.3% PTA in water	Not reported
(De Greef et al., 2015)	Human	Cadaver; age not reported	Middle ear	3 wt% PTA in water	48 hr
(Disney et al., 2017)	Cow	Not reported	Intervertebral disc	Reported to follow Metscher, 2009a	14 days
(Dullin et al., 2017)	Mouse	Adult	Heart	0.7% PTA in 70% ethanol	6 days
(Dullin et al., 2017)	Mouse	E12, E15, E18, P0, P2 and P5	Whole body	0.7% PTA in 70 % ethanol	4–12 days
(Dunmore-Buyze et al., 2014)	Mouse	Adult	Heart	5% PTA in deionized water	Perfusion for 30 min
(Faulwetter et al., 2012)	Marine invertebrate spp.	Not reported	Whole body	0.3% PTA in 70% ethanol	Overnight – 5 days
(Kaucka et al., 2017)	Mouse	E12.5, E15.5, E16.5, and E17.5	E12.5 and 15.5 – whole body E16.5 and 17.5 – decapitated head	0.5–1.0% PTA in 90% methanol	E12.5 – 4 days E15.5 – 6 days E16.5 and 17.5 – 9–15 days
(Kaucka et al., 2018)	Mouse	E12.5, E15.5, and E18.5	Whole body	1.0–1.5% PTA in 90% methanol	E12.5 – 7 days E15.5 – 3 weeks E18.5 – 7 weeks
(Krings et al., 2017)	Tadpole	Not reported	Whole body	0.3% PTA in 70% ethanol	Overnight
(Missbach-Guentner et al., 2018)	Mouse	Adult	Kidney	Transcardial perfusion of 5% PTA in water followed by immersion in 0.7% PTA in 70% ethanol and 4% PFA	4–18 days
(Nieminen et al., 2015)	Horse	Adult	Joints and articular cartilage	1% w/v PTA in 70% ethanol	Up to 270 hr
(Nierenberger et al., 2015)	Pig	Not reported	Iliac vein	0.3% PTA in 70% ethanol	Overnight
(Pauwels et al., 2013)	Mouse	Adult	Hind limb, skin removed	50% PTA in deionized water (10g in 20 mL)	24 hr – 1 wk
(Shearer et al., 2014)	Pig	Not reported	Ligament and tendon	0.3% PTA in 70% ethanol	15–150 hr
(Smith et al., 2016)	Bumblebee	4 day	Head	0.5% PTA in 70% ethanol	1–9 days
(Swart et al., 2016)	Blue bottle fly	Adult	Head and thorax	0.5% PTA	3–7 days
(Tesařová et al., 2016)	Mouse	E15.5 embryo	Whole body	0.7% PTA in 90% methanol	6 days

Table 3.

Duration for PTA staining based on age and strain.

	PTA Staining Time	
Age	**C57BL/6J Background**	**CD1 Background**
E13.5 (full embryo)	5 days	Not tested
E14.5 (full embryo)	6 days	11 days
E15.5 (full embryo)	7 days	12 days
E16.5 (head and upper thorax)	8 days	8 days
E17.5 (head and upper thorax)	12 days	18 days
P0 (head only, skin removed)	14 days	Not tested
P7 (head only, skin removed)	20 days	Not tested

Table 4.

Typical μCT scan settings by age. These settings provided excellent visualization of even the thinnest layers of differentiated soft tissue.

Age	Tube Size	kV	μA	Average Voxel Size (mm)
E13.5	180	60	170	0.005
E14.5	180	60	170	0.005
E15.5	180	60–80	100–170	0.0055
E16.5	180	60–80	120–170	0.006
E17.5	180	80	160	0.0065
P0	300	80	75	0.007
P7	300	100	100	0.011